Electronic structures of hexagonal RMnO$_3$ (R=Gd, Tb, Dy, and Ho) thin films: Optical spectroscopy and first-principles calculations

Woo Seok Choi,[1] Dong Geun Kim,[2] Sung Seok A. Seo,[1] Soon Jae Moon,[1] Daesu Lee,[1] Jung Hyuk Lee,[1] Ho Sik Lee,[2]
Deok-Yong Cho,[2] Yun Sang Lee,[3] Pattukkannu Murugavel,[1] Jaejun Yu,[2] and Tae W. Noh[1,*]

[1]*ReCOE & FPRD, Department of Physics and Astronomy, Seoul National University, Seoul 151-747, Korea*
[2]*CSCMR, Department of Physics and Astronomy, Seoul National University, Seoul 151-747, Korea*
[3]*Department of Physics, Soongsil University, Seoul 156-743, Korea*

We investigated the electronic structure of multiferroic hexagonal RMnO$_3$ (R=Gd, Tb, Dy, and Ho) thin films using both optical spectroscopy and first-principles calculations. One of the difficulties in explaining the electronic structures of hexagonal RMnO$_3$ is that they exist in nature with limited rare earth ions (i.e., R=Sc, Y, and Ho-Lu), so a systematic study in terms of the different R ions has been lacking. Recently, our group succeeded in fabricating hexagonal RMnO$_3$ (R=Gd, Tb, and Dy) using the epitaxial stabilization technique [Adv. Mater. (Weinheim Ger.) **18**, 3125 (2006)]. Using artificially stabilized hexagonal RMnO$_3$, we extended the optical spectroscopic studies on the hexagonal multiferroic manganite system. We observed two optical transitions located near 1.7 and 2.3 eV, in addition to the predominant absorption above 5 eV. With the help of first-principles calculations, we attributed the low-lying optical absorption peaks to interband transitions from the oxygen states hybridized strongly with different Mn orbital symmetries to the Mn $3d_{3z^2-r^2}$ state. As the ionic radius of the rare earth ion increased, we observed a systematic increase of the lowest peak position, which became more evident when compared with previously reported results. We explained this systematic change in terms of a flattening of the MnO$_5$ triangular bipyramid.

I. INTRODUCTION

Multiferroic oxides have attracted considerable recent attention due to their intriguing coupling between the magnetic and electric order parameters.[1–10] This magnetoelectric coupling in a single material could lead to new applications, and new understanding of the underlying physics involved. Of all the known multiferroic materials, the RMnO$_3$ rare-earth manganites attracted particular interest. These intriguing material systems have two kinds of crystal structure. Depending on the rare-earth ionic radius, they form either an orthorhombic phase (R=Bi and La-Dy) or a hexagonal phase (R=Sc, and Y, Ho-Lu). Due to the recent observations of very strong magnetoelectric coupling, there has been a flurry of investigations of orthorhombic RMnO$_3$.[5,6,11–14] However, orthorhombic RMnO$_3$ has relatively low ferroelectric and magnetic ordering temperatures that are often well below the temperature of liquid nitrogen.[5,6,11]

Hexagonal RMnO$_3$ (hexa-RMnO$_3$) have ferroelectric properties with fairly large remnant polarization and quite high Curie temperature (T_C), typically above 590 K. They also exhibit antiferromagnetic behaviors, but their Néel temperature (T_N) is quite low, in the range of 70–120 K, probably due to geometrical frustration.[7] Their magnetoelectric couplings were reported to be smaller than those of orthorhombic RMnO$_3$.[7,8] However, such couplings have been clearly identified in the ferroelectric and antiferromagnetic phases.[7–9,15–17] For example, the magnetic ordering in hexa-RMnO$_3$ can be controlled by a static electric field[7] or the static dielectric constant shows anomalies when an external magnetic field is applied.[15,16]

To understand the physics involved in these multiferroic materials, it is necessary to understand their electronic struc-

ture. Compared to orthorhombic RMnO$_3$,[18,19] the detailed electronic structure of hexa-RMnO$_3$ is not very well understood. There have been attempts using first-principles calculations,[20,21] optical spectroscopy,[10,22] x-ray absorption spectroscopy,[23] photoemission spectroscopy (PES),[24] and second harmonic generation studies.[25] Despite these efforts, controversy remains over the origins of the energy bands of hexa-RMnO$_3$ near the Fermi surface.[21,22,24,25]

One of the difficulties in understanding the electronic structure of hexa-RMnO$_3$ is the absence of any systematic link between the physical properties and tuning parameters. For example, in the bulk hexa-RMnO$_3$ phase, the T_C and T_N values do not show a systematic variation with the radius of the R ion.[26,27] Furthermore, all of the optical conductivity spectra $\sigma(\omega)$ of the bulk hexa-RMnO$_3$ show interband optical transitions located nearly at the same frequencies.[10,22] In this sense, it is quite worthwhile to study hexa-RMnO$_3$ by synthesizing the metastable hexagonal phases of manganites to search for possible variations in electronic structure. Recently, our group successfully fabricated thin films of hexa-RMnO$_3$ [R=Gd,[28] Tb,[9,29] and Dy (Ref. [30])] using the epitaxial stabilization (epistabilization) technique.[31] This film fabrication technique opened the way to fabricating new multiferroic materials as well as extending the phase diagrams of hexa-RMnO$_3$ phases. We also found that significant variations in physical properties exist in synthesized hexa-RMnO$_3$ thin films.

In this paper, we report on the systematic changes in the electronic structure of the hexa-RMnO$_3$ (R=Gd, Tb, Dy, and Ho) thin films with variation of the rare-earth ions using optical spectroscopy and first-principles calculations. Optical spectroscopy has been a powerful tool for investigating the

systematic electronic band structure of solids.[32,33] We found that $\sigma(\omega)$ of the hexa-RMnO$_3$ films is qualitatively similar to that of the bulk hexa-RMnO$_3$ (i.e., R=Lu and Y), including the interband transitions.[10,22] However, the lowest peak shows a systematic trend, i.e., an increase in peak energy with the increase in R ionic radius. Combined with the results of first-principles calculations, we attribute this systematic change to the change of crystal field energy linked to the ionic radius of the R ion. This shows that local crystal distortion could play an important role in changing the electronic structure of the multiferroic hexagonal phases.

II. EXPERIMENTAL AND THEORETICAL METHODS

A. Film fabrication

We used pulsed laser deposition techniques to fabricate high-quality hexa-RMnO$_3$ (R=Dy, Tb, Gd, and Ho), and half-substituted (Dy,Ho)MnO$_3$ and (Tb,Ho)MnO$_3$ thin films. Note that in bulk form, DyMnO$_3$, TbMnO$_3$, and GdMnO$_3$ have orthorhombic phases. We used the epistabilization technique to convert these materials into hexagonal form. We grew them in the hexagonal phases by depositing the films on single crystalline yttria-stabilized zirconia (YSZ)(111) substrates. [Note that for transmission studies, we used YSZ(111) single crystals polished on both sides as substrates.] Since the atomic arrangements of the substrate surfaces form hexagonal nets, the metastable hexa-RMnO$_3$ phase could be formed by maintaining the coherent film-substrate interface and minimizing the surface energy.[31] Using x-ray diffraction (XRD) measurements, we confirmed that all of the thin films were grown epitaxially with their c axis perpendicular to the film surface. The thickness of the films was around 70 nm. We could observe partial relaxation of our hexa-RMO$_3$ thin films at this thickness, although the crystal structure did not change to affect the qualitative electronic structure. The partial relaxation might be possibly due to quite noticeable mismatch between the thin film and the substrate. More details about the growth condition and structural characterization of the thin films are published elsewhere.[9,28–30]

B. Optical measurements

We obtained near-normal-incident reflectance and transmittance spectra of the thin films in the photon energy range of 0.1–6.0 eV. We used a Fourier transform infrared spectrometer (Bruker IFS66v/S) and a grating-type spectrophotometer (CARY 5G) at 0.1—1.2 and 0.4–6.0 eV, respectively. Figure 1 shows the optical spectra of a hexa-TbMnO$_3$ thin film (solid lines) and a YSZ(111) bare substrate (dashed lines). The thick blue and thin red lines represent the transmittance and reflectance spectra, respectively. Since the band-gap edge of the YSZ(111) substrate is located near 5 eV, we were able to obtain meaningful transmittance spectra up to that level. In the spectral range of 0.15–5.0 eV, we could determine the in-plane $\sigma(\omega)$ of the hexa-RMnO$_3$ thin films from the transmittance and reflectance spectra using a numerical iteration process called the intensity transfer matrix method.[34]
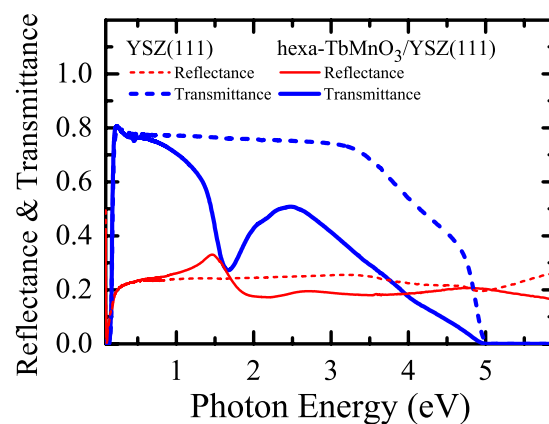
FIG. 1. (Color online) Optical spectra of YSZ(111) substrate (dashed lines) and hexagonal TbMnO$_3$ thin film (solid lines) artificially fabricated on YSZ(111) substrate using the epitaxial stabilization technique. Reflectance and transmittance spectra are shown as the thin red and thick blue lines, respectively.

C. First-principles calculations

We performed first-principles calculations for YMnO$_3$ since its structural parameters have been sufficiently studied for the theoretical calculations.[35] To deal with the effects of strong Coulomb interactions among 3d electrons, we used the local density approximation (LDA)+U methods based on density functional theory, as implemented in a linear-combination-of-localized-pseudo-atomic-orbital (LCPAO) code.[36–40] We used the effective on-site Coulomb energy parameter $U_{eff,Mn}$=4 eV for Mn 3d, which turned out to be suitable for describing the band gap and magnetic properties of MnO.[36] We used Troullier-Martins-type norm-conserving pseudopotentials to replace the deep core potentials. The calculation unit cell contains 6 f.u. of hexa-RMnO$_3$. For numerical integration and the solution of Poisson's equation, we used an energy cutoff of 240 Ry. For the k-space integrations, we used a $4\times4\times4$ grid. To describe the ground state spin-ordering appropriately, we performed noncollinear spin calculations including the spin-orbit coupling.

We also wanted to carry out first-principles calculations for the hexa-GdMnO$_3$. However, up to now, there have not been any detailed structural studies on hexa-GdMnO$_3$, so we had to make the following approximation. To include the atomic positions of GdMnO$_3$ in the calculation, we used experimental neutron diffraction data for YMnO$_3$,[35] but putting the Gd ions in the place of the Y ions. For the Gd 4f electrons, we used $U_{eff,Gd}$=6 eV. We found that the positions of f-electron energy levels are located at about 8 eV below and 10 eV above the Fermi level, indicating that the effects of f electrons on the valence electronic structure could be considered as minimal. For both YMnO$_3$ and GdMnO$_3$, the electronic structures related to the Mn 3d and O 2p manifolds showed nearly identical features near the Fermi level. Therefore, the first-principles calculation results of YMnO$_3$ should be sufficient for understanding detailed electronic structures of hexa-RMnO$_3$ near the Fermi level.
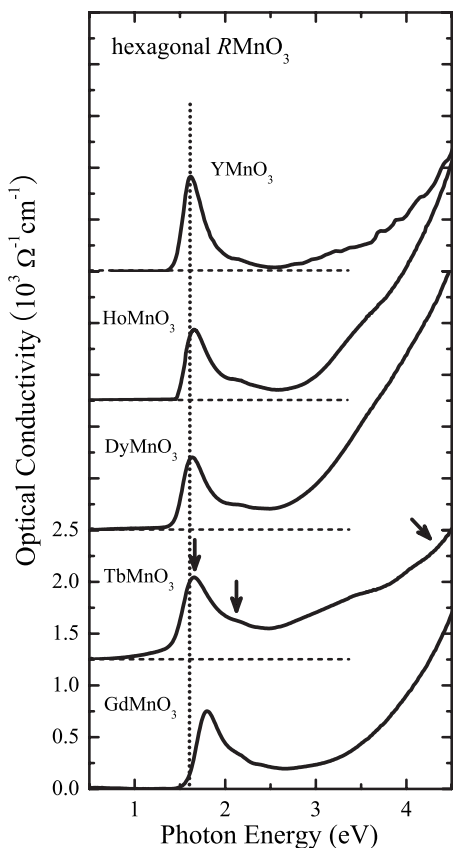
FIG. 2. Optical conductivity spectra of hexagonal HoMnO$_3$, DyMnO$_3$, TbMnO$_3$, and GdMnO$_3$ thin films. For the sake of comparison, the reported spectrum of bulk YMnO$_3$ (Ref. 22) is also shown. For clarity, the spectra have been plotted with offsets of 1250 Ω^{-1} cm^{-1} vertically between each curve, and the base line for each curve is shown by the horizontal dashed line. The arrows in the TbMnO$_3$ spectrum indicate the three peak positions where optical absorption occurs. The vertical dotted line indicates the first optical transition peak position of YMnO$_3$.

III. RESULTS AND DISCUSSION

A. Generic spectral features of hexagonal RMnO$_3$

Figure 2 shows the in-plane $\sigma(\omega)$ of hexa-RMnO$_3$ (R =Gd, Tb, Dy, and Ho) thin films. Note that the hexa-GdMnO$_3$, TbMnO$_3$, and DyMnO$_3$ films were artificially fabricated using the epistabilization technique. For the sake of comparison, $\sigma(\omega)$ of single crystal YMnO$_3$ is also shown.[22] The overall spectral shapes of the thin films and the bulk sample are similar. (Note that similar optical spectra were also reported in the literature for the other bulk hexa-RMnO$_3$.[10,22]) This similarity suggests that our epistabilized hexa-RMnO$_3$ thin films should have a similar electronic structure to that of the bulk hexa-RMnO$_3$.

Up to this point, $\sigma(\omega)$ of bulk RMnO$_3$ (R=Sc, Lu, Er, and Y) has been interpreted in terms of two absorption peaks. However, we noted that TbMnO$_3$ has three important spectral features, which are indicated by arrows in Fig. 2. Note that the second peak near 2.3 eV in $\sigma(\omega)$ of YMnO$_3$ is not very clear due to relatively large noise level caused from

reflectance measurements on the single crystal sample. However, it is quite well known that transmittance measurements used for the thin films are much more sensitive than the reflectance measurements used for the bulk samples. Since we used transmittance measurements, where the nonreproducibility effects were smaller than 1%, we could evidently observe the second peak. Thus, we can state that hexa-RMnO$_3$ compounds have three important spectral absorption peak features: a sharp peak near 1.7 eV, a weak peak near 2.3 eV, and the most prominent peak located higher than 5 eV.

Another notable point is that the position of the first peak shows a systematic change between 1.61 and 1.81 eV, depending on the R ion. The vertical dotted line in Fig. 2 indicates the first peak position of YMnO$_3$. As the radius of the R ion increases from Y to Gd, the position of the first peak shifts to higher energy. The shift in peak position becomes significant for artificially fabricated hexa-RMnO$_3$ films, especially hexa-GdMnO$_3$. The systematic change of the sharp optical transition peak in hexa-RMnO$_3$ implies that there should be systematic variations in their electronic structures depending on the radius of the R ion.

B. Attribution of the optical absorption peaks

There has been debate on the origin of the sharp optical transition at ~1.7 eV. One interpretation is that it comes from the charge transfer transition from the O $2p$ to the Mn $3d$ states.[21,22,24] An earlier PES study suggested that the highest occupied level has mainly O $2p$ character, while the unoccupied level has Mn $3d$ character.[24] Other Mn $3d$ states in the valence band are located at much lower energy, so that they cannot contribute to the optical transition at ~1.7 eV. The other interpretation is that it comes from the on-site d-d transition between the Mn $3d$ levels.[10,25] Hexa-RMnO$_3$ has a Mn-O triangular bipyramid cage, so two e_{1g} orbitals (d_{yz} and d_{zx}) form the lowest level, followed by two e_{2g} orbitals (d_{xy} and $d_{x^2-y^2}$), and the a_{1g} orbital ($d_{3z^2-r^2}$), as shown in Fig. 5(a). In this simple atomic picture, the transition at ~1.7 eV could be attributed to the on-site d-d transition between the occupied e_{2g} orbitals and the unoccupied a_{1g} orbital. In principles, optical transitions between d orbitals are forbidden due to the selection rule for electric dipole transitions. However, in many transition metal oxide systems, strong hybridization between the oxygen $2p$ bands and transition metal d bands could allow this transition.[41]

Our LDA+U calculations for hexa-RMnO$_3$ electronic structures provide insights into the O $2p$-Mn $3d$ transition versus on-site d-d transition discussion. We found that the calculated results for GdMnO$_3$ were quite similar to those for YMnO$_3$, so we will explain the calculation results in detail only for YMnO$_3$. Figure 3 shows the orbital-resolved density of state (DOS) of YMnO$_3$. The unoccupied manganese $d_{3z^2-r^2}$ state is located just ~1 eV above the Fermi level. On the other hand, for the occupied states near −2 eV, the in-plane O $2p$ and all Mn d orbitals except for $d_{3z^2-r^2}$ orbital contribute together. These states can be interpreted in terms of two hybridized states between in-plane O $2p$ orbitals with the associated Mn d orbitals. The dashed blue line shows Mn
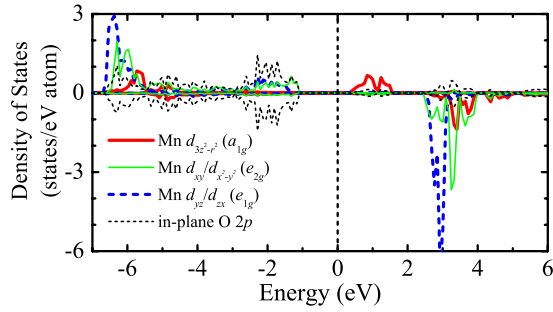
FIG. 3. (Color online) Orbital-resolved densities of states of Mn 3d orbitals and the in-plane O 2p orbital for YMnO$_3$.

DOS with the Mn d_{yz} and d_{zx} orbitals. This state is hybridized with the in-plane O 2p orbitals forming a state with d_{yz}/d_{zx} symmetry. On the other hand, the solid green line shows Mn DOS with the Mn d_{xy} and $d_{x^2-y^2}$ orbitals. This state is also hybridized with the in-plane O 2p orbitals forming a state with $d_{xy}/d_{x^2-y^2}$ symmetry. Note that the Mn DOS of the state with d_{yz}/d_{zx} symmetry is located at somewhat lower energy than that with $d_{xy}/d_{x^2-y^2}$ symmetry.

This calculated electronic structure explains the three spectral features in Fig. 2 quite well. Taking into account the energy levels in Fig. 3, the sharp first absorption peak at ~1.7 eV can be attributed to the interband optical transition from the occupied hybridized O 2p state with the $d_{xy}/d_{x^2-y^2}$ orbitals to the unoccupied Mn $d_{3z^2-r^2}$ state. Similarly, the weak second peak at ~2.3 eV can be attributed to the interband optical transition from the occupied hybridized O 2p state with the d_{yz}/d_{zx} orbitals to the unoccupied Mn $d_{3z^2-r^2}$ state. The strong third peak above 5 eV is the sum of two interband transitions: one from the broad O 2p states at ~−4 eV to the Mn $d_{3z^2-r^2}$ state, and the other from the O 2p states at ~−2 eV to the Mn 3d states with various orbitals at ~3 eV. In these assumptions, it is worth pointing out that the minute structure near 2.3 eV, which was hardly discernible in the previous studies of the bulk samples, can be appropriately attributed. The agreement between the experimental spectroscopy data and the theoretical explanations indicates that first-principles calculation results do represent the electronic structure of the multiferroic hexa-RMnO$_3$ quite reliably.

Our investigations revealed that hybridization could play a crucial role in the electronic structure of hexa-RMnO$_3$ materials. To date, the optical transitions that involve an empty d-electronic state have been attributed to either d-d or p-d transitions. Such simple interpretations are not suitable for explaining the electronic structure of hexa-RMnO$_3$ materials. As shown in Fig. 3, the occupied states that are responsible for the peaks at ~1.7 and ~2.3 eV come from the strong hybridization between the O 2p and the related Mn 3d orbitals. Due to the strong hybridized nature of the occupied states, we cannot attribute the optical transition in the hexagonal phase simply to strict d-d or p-d transitions. Instead, the optical transitions in hexa-RMnO$_3$ should be regarded as an interband charge transfer excitation from the oxygen states strongly hybridized with associated Mn orbital symmetries to the Mn 3$d_{3z^2-r^2}$ state.
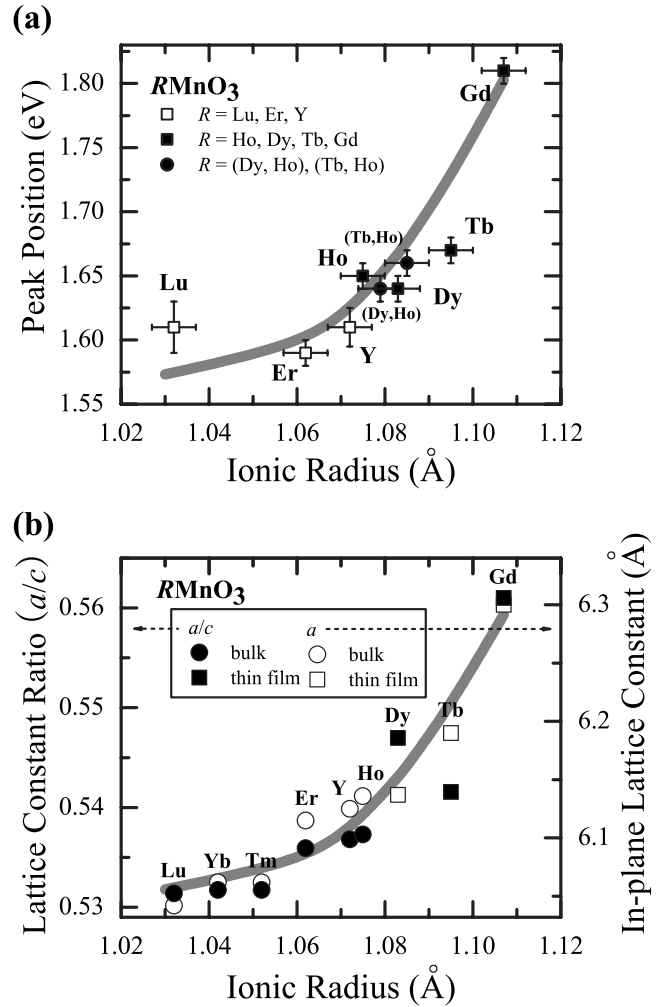
FIG. 4. (a) Peak positions of the optical transition peak at ~1.7 eV for numerous hexagonal RMnO$_3$. Empty squares denote the peak positions of the bulk hexagonal RMnO$_3$ [R=Lu (Ref. 10), Er, and Y (Ref. 22)], whereas filled squares denote those of the thin film hexagonal RMnO$_3$ (R=Dy, Tb, and Gd). Filled circles denote the peak positions of the half-substituted hexagonal RMnO$_3$ thin films [R=(Dy$_{0.5}$Ho$_{0.5}$) and (Tb$_{0.5}$Ho$_{0.5}$)]. (b) The lattice constant ratio (a/c, filled symbols) and the in-plane lattice constant (a, empty symbols) of bulk hexagonal RMnO$_3$ [circles, R=Lu, Yb, Tm, Er, Y, and Ho (Ref. 42)], and film hexagonal RMnO$_3$ (squares, R=Dy, Tb, and Gd). The thick gray lines in both (a) and (b) are included simply as visual aids.

C. Systematic shift of the interband optical transition peak at ~1.7 eV

We now discuss the systematic shift of the optical transition peak at ~1.7 eV depending on the R ion in hexa-RMnO$_3$. Figure 4(a) shows the peak position as a function of the radius of the R ion. For clarity, we have also included the peak positions for the bulk hexa-RMnO$_3$ samples from the literatures[10,22] and the peak positions of artificially fabricated half-substituted (Dy,Ho)MnO$_3$ and (Tb,Ho)MnO$_3$ thin films. Except for the small deviations for LuMnO$_3$ and HoMnO$_3$, an increase in the peak position according to the increase in radius of the R ion is clearly visible. Note that the

peak position of the hexagonal manganite with the largest R ion among this series, i.e., GdMnO$_3$, is very high, reaching 1.81 eV. This value is higher by $\sim$0.2 eV than those of usual bulk hexa-RMnO$_3$, which typically have peak positions around 1.6 eV.

We looked for physical properties that could be related to the observed changes in peak position. Figure 4(b) shows the systematic variation in the lattice constant ratio a/c and the in-plane lattice constant a for hexa-RMnO$_3$. The lattice constant values of the bulk samples are taken from the literature,[42] whereas the values of the thin film samples were obtained from our XRD measurements. These two structural quantities increase as a function of the ionic radius of the R ion, similar to the R ionic radius dependence of the $\sim$1.7 eV peak position. [Although not shown here, we also found that the c-axis lattice constant remains nearly the same, unrelated to the R ionic radius.] This indicates that the change in the electronic structure of hexa-RMnO$_3$ should be closely related to the structural changes.

D. Possible origin of the ∼1.7 eV peak shift

To explain the close relationship between the change in the first peak position and variations in the structural properties, we looked at how structural changes might affect the energy levels of hexa-RMnO$_3$ in an atomic picture. Although such a simple picture cannot take into account all of the strong hybridization effects, it can still provide some insight into the relationship between the structure and energy bands. Figure 5(a) shows the configuration of the Mn-O triangular bipyramid and associated energy level diagram for Mn $3d$ electrons. If we assume that the c-axis lattice constant remains fixed as we increase the radius of the R ion, the MnO$_5$ triangular bipyramid will flatten out. Then, due to the crystal field splitting, the energy level of the Mn $d_{3z^2-r^2}$ state should increase significantly, while the Mn $d_{xy}/d_{x^2-y^2}$ state would change only very little. Therefore, the optical transition from the Mn $d_{xy}/d_{x^2-y^2}$ state to the Mn $d_{3z^2-r^2}$ state will shift to higher energy as the radius of the R ion increases. This simple atomic picture can explain the systematic increase of the first optical peak with increase of R ionic radius.

As we showed in Sec. III B, the energy bands just below the Fermi surface should have very strong hybridizations between O $2p$ and the related Mn $3d$ orbitals. To take into account these hybridization effects appropriately, we relied on our first-principles calculations. To address the relationship between the electronic structure and the MnO$_5$ triangular bipyramid flattening, we calculated the DOS for a hypothetical material system that has the same crystal structure as that of YMnO$_3$ but with a 2% reduction in spacing between the Mn and the apical oxygen ions.[43] Figure 5(b) shows the DOS of the strongly hybridized Mn $d_{3z^2-r^2}$ state for normal YMnO$_3$ and YMnO$_3$ with the MnO$_5$ triangular bipyramid flattened by 2%. There are little changes in the associated DOS below the Fermi level, but the unoccupied Mn $d_{3z^2-r^2}$ energy level moves by 0.24 eV to higher energy. [We found that there are few changes in the DOS of Mn $3d$ orbitals with other symmetries. The energy levels of d_{yz} and d_{zx} orbitals changed little in our calculation results, although they should also

(a) MnO$_5$ triangular bipyramid
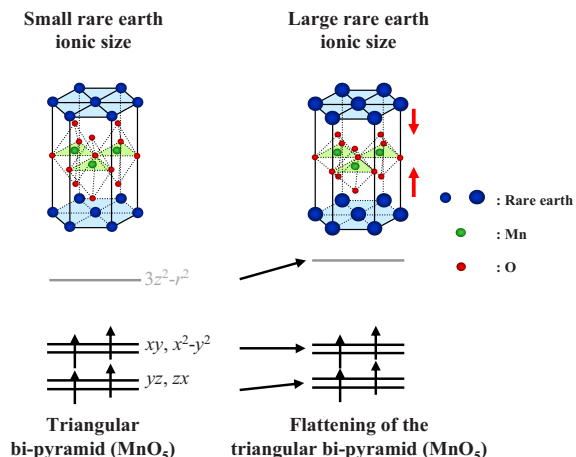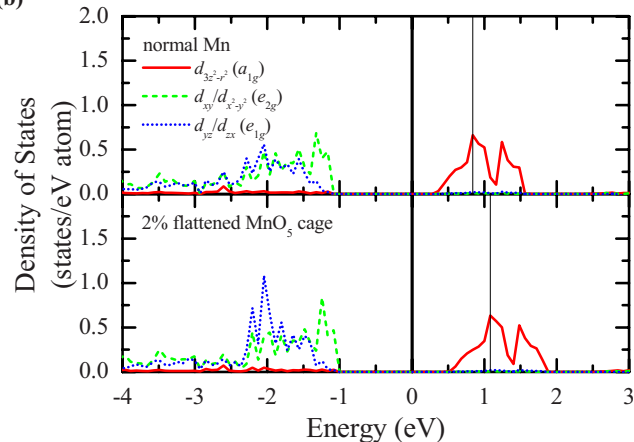
FIG. 5. (Color online) (a) Schematic representation of the crystal field splitting changes due to flattening of the MnO$_5$ triangular bipyramid. The flattening occurs due to the increase of the rare-earth ionic radius with the fixed c-axis lattice constant. As the flattening occurs, due to the orbital symmetries, the $d_{3z^2-r^2}$ orbital will shift to higher energy, whereas the d_{xy} and $d_{x^2-y^2}$ orbitals stay the same. (b) First-principles calculation results for the Mn orbital DOS of YMnO$_3$ without and with flattening of the triangular bipyramid (results are shown only for up spins). The calculations took into account the hybridization between the in-plane O $2p$ and associated Mn $3d$ orbitals. When the spacing between the Mn and the apical oxygen ions is reduced by 2%, the DOS for the unoccupied Mn $d_{3z^2-r^2}$ orbital state shows an upward shift of 0.24 eV, whereas the changes for other orbital states are relatively small.

increase to a little higher energy due to their z symmetry.] These theoretical results explain the observed increase of the first peak from about 1.6 to 1.8 eV. Therefore, the observed spectral position changes in Fig. 4(a) should come from the flattening of the MnO$_5$ triangular bipyramid in the hexa-RMnO$_3$ structure.

IV. SUMMARY

We investigated the optical conductivity spectra of artificially fabricated hexagonal RMnO$_3$ (R=Gd, Tb, Dy, and Ho)

thin films using optical spectroscopy and first-principles calculations. We were able to characterize the optical transition comprehensively by comparing the experimental and theoretical results. From our first-principles calculation results, we suggested that the Mn $3d$ states just below the Fermi energy had strong hybridized characteristics between the O $2p$ and the associated Mn $3d$ orbitals. We further observed a systematic increase in the lowest optical transition at ~ 1.7 eV with an increase in the R ionic radius. From these studies, we concluded that the electronic structure of the hexagonal RMnO$_3$ should have a close relationship to the crystal structure, especially the distance between Mn and apical O ions in the MnO$_5$ triangular bipyramid. Investigations of other physical properties of the artificially fabricated hexago-

nal RMnO$_3$ could enhance our understanding of the intriguing multiferroic manganite system.

*twnoh@snu.ac.kr

[1] W. Eerenstein, N. D. Mathur, and J. F. Scott, Nature (London) **442**, 759 (2006).

[2] N. A. Spaldin and M. Fiebig, Science **309**, 391 (2005).

[3] R. Ramesh and N. A. Spaldin, Nat. Mater. **6**, 21 (2007).

[4] N. Hur, S. Park, P. A. Sharma, J. S. Ahn, S. Guha, and S. W. Cheong, Nature (London) **429**, 392 (2004).

[5] T. Kimura, T. Goto, H. Shintani, K. Ishizaka, T. Arima, and Y. Tokura, Nature (London) **426**, 55 (2003).

[6] T. Goto, T. Kimura, G. Lawes, A. P. Ramirez, and Y. Tokura, Phys. Rev. Lett. **92**, 257201 (2004).

[7] Th. Lottermoser, Th. Lonkai, U. Amann, D. Hohlwein, J. Ihringer, and M. Fiebig, Nature (London) **430**, 541 (2004).

[8] M. Fiebig, Th. Lottermoser, D. Frohlich, A. V. Goltsev, and R. V. Pisarev, Nature (London) **419**, 818 (2002).

[9] Jung-Hyuk Lee, Pattukkannu Murugavel, Hyejin Ryu, Daesu Lee, Ji Young Jo, Jae Wook Kim, Hyung Jin Kim, Kee Hoon Kim, Younghun Jo, Myung-Hwa Jung, Young Hwa Oh, Young-Woon Kim, Jong-Gul Yoon, Jin-Seok Chung, and Tae Won Noh, Adv. Mater. (Weinheim, Ger.) **18**, 3125 (2006).

[10] A. B. Souchkov, J. R. Simpson, M. Quijada, H. Ishibashi, N. Hur, J. S. Ahn, S. W. Cheong, A. J. Millis, and H. D. Drew, Phys. Rev. Lett. **91**, 027203 (2003).

[11] T. Kimura, G. Lawes, T. Goto, and Y. Tokura, A. P. Ramirez, Phys. Rev. B **71**, 224425 (2005).

[12] T. Arima, T. Goto, Y. Yamasaki, S. Miyasaka, K. Ishii, M. Tsubota, T. Inami, Y. Murakami, and Y. Tokura, Phys. Rev. B **72**, 100102(R) (2005).

[13] M. Kenzelmann, A. B. Harris, S. Jonas, C. Broholm, J. Schefer, S. B. Kim, C. L. Zhang, S.-W. Cheong, O. P. Vajk, and J. W. Lynn, Phys. Rev. Lett. **95**, 087206 (2005).

[14] N. Aliouane, D. N. Argyriou, J. Strempfer, I. Zegkinoglou, S. Landsgesell, and M. v. Zimmermann, Phys. Rev. B **73**, 020102(R) (2006).

[15] F. Yen, C. R. dela Cruz, B. Lorenz, Y. Y. Sun, Y. Q. Wang, M. M. Gospodinov, and C. W. Chu, Phys. Rev. B **71**, 180407(R) (2005).

[16] B. Lorenz, A. P. Litvinchuk, M. M. Gospodinov, and C. W. Chu, Phys. Rev. Lett. **92**, 087204 (2004).

[17] O. P. Vajk, M. Kenzelmann, J. W. Lynn, S. B. Kim, and S.-W. Cheong, Phys. Rev. Lett. **94**, 087601 (2005).

[18] Y. Tokura and N. Nagaosa, Science **288**, 462 (2000).

[19] M. W. Kim, S. J. Moon, J. H. Jung, J. J. Yu, S. Parashar, P. Murugavel, J. H. Lee, and T. W. Noh, Phys. Rev. Lett. **96**, 247205 (2006).

[20] B. B. van Aken, T. T. M. Palstra, A. Filippetti, and N. A. Spaldin, Nat. Mater. **3**, 164 (2004).

[21] J. E. Medvedeva, V. I. Anisimov, M. A. Korotin, O. N. Mryasov, and A. J. Freeman, J. Phys.: Condens. Matter **12**, 4947 (2000).

[22] A. M. Kalashnikova and R. V. Pisarev, JETP Lett. **78**, 143 (2003).

[23] D. Y. Cho, J.-Y. Kim, B.-G. Park, K.-J. Rho, J.-H. Park, H.-J. Noh, B. J. Kim, S.-J. Oh, H.-M. Park, J.-S. Ahn, H. Ishibashi, S.-W. Cheong, J. H. Lee, P. Murugavel, T. W. Noh, A. Tanaka, and T. Jo, Phys. Rev. Lett. **98**, 217601 (2007).

[24] J.-S. Kang, S. W. Han, J.-G. Park, S. C. Wi, S. S. Lee, G. Kim, H. J. Song, H. J. Shin, W. Jo, and B. I. Min, Phys. Rev. B **71**, 092405 (2005).

[25] C. Degenhardt, M. Fiebig, D. Froehlich, Th. Lottermoser, and R. V. Pisarev, Appl. Phys. B: Lasers Opt. **73**, 139 (2001).

[26] Th. Lonkai, D. G. Tomuta, U. Amann, J. Ihringer, R. W. Hendrikx, D. M. Toebbens, and J. A. Mydosh, Phys. Rev. B **69**, 134108 (2004).

[27] J.-S. Zhou, J. B. Goodenough, J. M. Gallardo-Amores, E. Morán, M. A. Alario-Franco, and R. Caudillo, Phys. Rev. B **74**, 014422 (2006).

[28] D. Lee, J. H. Lee, P. Murugavel, S. Y. Jang, T. W. Noh, Y. Jo, M. H. Jung, Y. D. Ko, and J. S. Chung, Appl. Phys. Lett. **90**, 182504 (2007).

[29] J.-H. Lee, D. Lee, T. W. Noh, P. Murugavel, J. W. Kim, K. H. Kim, Y. Jo, M.-H. Jung, J.-G. Yoon, and J.-S. Chung, J. Mater. Res. **22**, 2156 (2007).

[30] J.-H. Lee, P. Murugavel, D. Lee, T. W. Noh, Y. Jo, M. H. Jung, K. H. Jang, and J. G. Park, Appl. Phys. Lett. **90**, 012903 (2007).

[31] A. A. Bosak, C. Dubourdieu, J.-P. Sénateur, O. Y. Gorbenko, and A. R. Kaul, Cryst. Eng. **5**, 355 (2002).

[32] S. J. Moon, M. W. Kim, K. W. Kim, Y. S. Lee, J.-Y. Kim, J.-H. Park, B. J. Kim, S.-J. Oh, S. Nakatsuji, Y. Maeno, I. Nagai, S. I. Ikeda, G. Cao, and T. W. Noh, Phys. Rev. B **74**, 113104 (2006).

[33] W. S. Choi, S. S. A. Seo, K. W. Kim, T. W. Noh, M. Y. Kim, and S. Shin, Phys. Rev. B **74**, 205117 (2006).

[34] T. W. Noh, P. H. Song, S.-I. Lee, D. C. Harris, J. R. Gaines, and

J. C. Garland, Phys. Rev. B **46**, 4212 (1992).

[35] S. Lee, A. Pirogov, J. H. Han, J. G. Park, A. Hoshikawa, and T. Kamiyama, Phys. Rev. B **71**, 180413(R) (2005).

[36] M. J. Han, T. Ozaki, and J. Yu, Phys. Rev. B **73**, 045110 (2006).

[37] T. Ozaki and H. Kino, J. Chem. Phys. **121**, 10879 (2004).

[38] T. Ozaki, Phys. Rev. B **67**, 155108 (2003).

[39] T. Ozaki and H. Kino, Phys. Rev. B **69**, 195113 (2004).

[40] T. Ozaki and H. Kino, Phys. Rev. B **72**, 045121 (2005).

[41] See, for example, J. S. Lee, Y. S. Lee, T. W. Noh, K. Char, Jonghyurk Park, S.-J. Oh, J.-H. Park, C. B. Eom, T. Takeda, and R. Kanno, Phys. Rev. B **64**, 245107 (2001).

[42] H. L. Yakel, W. C. Koehler, E. F. Bertaut, and E. F. Forrat, Acta Crystallogr. **16**, 957 (1963).

[43] The 2% is calculated from the approximate amount of change in the lattice constant ratio (a/c) between YMnO$_3$ and GdMnO$_3$, as shown in Fig. 4(b).